

Solution-Processed n-Type Graphene Doping for Cathode in Inverted Polymer Light-Emitting Diodes

Sung-Joo Kwon,^{†,◆} Tae-Hee Han,^{‡,▽,¶,◆} Young-Hoon Kim,^{‡,⊥,◆} Towfiq Ahmed,[○] Hong-Kyu Seo,[†] Hobeom Kim,[‡] Dong Jin Kim,[§] Wentao Xu,^{‡,⊥} Byung Hee Hong,^{§,||} Jian-Xin Zhu,^{○,△} and Tae-Woo Lee^{*,‡,⊥,||}

[†]Department of Materials Science and Engineering, Pohang University of Science and Technology (POSTECH), Pohang, Gyungbuk 790-784, Republic of Korea

[‡]Department of Materials Science and Engineering, [§]Program in Nano Science and Technology, Graduate School of Convergence Science and Technology, ^{||}Department of Chemistry, [⊥]Research Institute of Advanced Materials, [#]BK21 PLUS SNU Materials Division for Educating Creative Global Leaders, Seoul National University, 1 Gwanak-ro Gwanak-gu, Seoul 08826, Republic of Korea

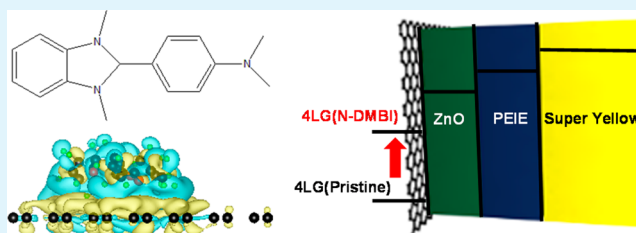
[▽]Department of Materials Science and Engineering and [¶]California NanoSystems Institute, University of California, Los Angeles, California 90095, United States

[○]Theoretical Division, [△]Center for Integrated Nanotechnologies, Los Alamos National Laboratory, Los Alamos, New Mexico 87545, United States

Supporting Information

ABSTRACT: n-Type doping with (4-(1,3-dimethyl-2,3-dihydro-1H-benzimidazol-2-yl)phenyl) dimethylamine (N-DMBI) reduces a work function (WF) of graphene by ~0.45 eV without significant reduction of optical transmittance. Solution process of N-DMBI on graphene provides effective n-type doping effect and air-stability at the same time. Although neutral N-DMBI act as an electron receptor leaving the graphene p-doped, radical N-DMBI acts as an electron donator leaving the graphene n-doped, which is demonstrated by density functional theory. We also verify the suitability of N-DMBI-doped n-type graphene for use as a cathode in inverted polymer light-emitting diodes (PLEDs) by using various analytical methods. Inverted PLEDs using a graphene cathode doped with N-DMBI radical showed dramatically improved device efficiency (~13.8 cd/A) than did inverted PLEDs with pristine graphene (~2.74 cd/A). N-DMBI-doped graphene can provide a practical way to produce graphene cathodes with low WF in various organic optoelectronics.

KEYWORDS: CVD graphene, chemical n-doping, transparent electrode, DFT calculation, PLED



1. INTRODUCTION

Graphene has been regarded as a potential material for flexible transparent conducting electrode to replace brittle indium–tin-oxide in optoelectronics due to its unique electrical and mechanical properties.^{1–8} Graphene has been used in various types of flexible organic optoelectronics including organic light-emitting diodes (OLEDs),^{9–17} organic photovoltaics,^{18–22} and organic thin-film transistors.^{23,24} Pristine graphene has work function (WF) of ~4.4 eV,^{6,7,15} and it forms large energy barrier from graphene electrode to overlying layers. Therefore, to facilitate charge carrier injection from electrode, energy level of graphene electrode should be appropriately aligned to remove large energy barrier between electrodes and adjacent organic materials. There have been several attempts to modify electrical properties of pristine graphene for use in organic optoelectronics. Among them, chemical doping has been considered as the most effective way to control these traits of pristine graphene.^{9–21,25–37} To use graphene as a cathode, n-type doping of pristine graphene is essentially required as well.

n-Type graphene doping is more challenging than p-type doping because transferred graphene film is inherently p-doped during wet transfer process of graphene films.^{38–40} Residual p-type dopants such as residues of catalytic metal etchant, polymer supporter (i.e., poly(methyl methacrylate) (PMMA)), and adsorbed H₂O or O₂ molecules in air act as p-type dopants for pristine graphene. Conventionally, n-doped graphene has been synthesized introducing nitrogen-containing molecules during the synthesis steps;^{25–28,30,36,37,41} this process introduces N atoms in the carbon networks. However, graphene synthesized by substitutional doping is not suitable for electrode applications because it inevitably causes structural disorder and opening of electronic band gap.^{25,26,36,37,41} N-containing gaseous molecules (e.g., NH₃, N₂H₄) have also been used for n-doped graphene, but chemical toxicity, volatility, and

Received: October 9, 2017

Accepted: January 11, 2018

Published: January 11, 2018

ineffective doping effect of N_2H_4 make it not suitable for ideal n-type dopants of graphene.^{26,30,31,42}

Standard structured OLEDs generally use low WF metal or their derivatives (e.g., Ca, Ba, CsCO_3 , LiF) as an electron injection layer formed using vacuum thermal evaporation, but they have suffered from severe air-instability of devices and high fabrication cost. To solve these issues, inverted structure of OLEDs have been proposed using air-stable and solution-processable metal oxide electron injection layers (e.g., ZnO, TiO_2 , NiOx).^{43–47} Graphene can be used as a cathode to fabricate flexible inverted OLEDs. Conventionally, chemical doping of pristine graphene for use of electrode in OLEDs mostly toward to p-type doping, which increases graphene's WF for anode application.^{8–12,15–17} To our best knowledge, previously reported n-doped graphene cathodes for inverted OLEDs employed thermal evaporation of Cs_2CO_3 on graphene,¹³ or substitutionally N-doped graphene.¹⁴ However, each approach has disadvantage of high fabrication cost with air-instability, and significant defect generation inside graphene cathode, respectively. To make efficient, stable and flexible inverted OLEDs with low fabrication cost, n-type doping method of pristine graphene that meets solution-processability, effective n-type doping without generating defects, and air-stability at the same time is essentially needed for practical flexible displays or solid-state lightings.

In this work, we used (4-(1,3-dimethyl-2,3-dihydro-1H-benzimidazol-2-yl)phenyl) dimethylamine (N-DMBI) as an n-type chemical dopant because it has effective n-type doping effect, air-stability, and solution-processability at the same time. N-DMBI has been reported as a strong and air-stable n-type dopant due to its strong electron donating capability when it forms radicals by thermal annealing.³² We verified the suitability of solution-processed n-type graphene doping that uses N-DMBI for use in inverted polymer light-emitting diodes (PLEDs) by using various types of analytical methods and theoretical calculation. Also, we fabricated inverted PLEDs using N-DMBI doped graphene cathode which has lower operating voltage and higher electroluminescent efficiency than those with pristine graphene.

2. EXPERIMENTAL SECTION

Single-layer graphene was synthesized on Cu foil by chemical vapor deposition. The foils were heated to 1060 °C with 15 sccm flow of H_2 gas and annealed for 30 min. As a carbon source, CH_4 gas was flowed at 60 sccm for 30 min. Then the foil was rapidly cooled to room temperature. The graphene on Cu foil, was covered with PMMA polymer solution (PMMA/chlorobenzene = 4.6 g/100 mL, purchased from Sigma-Aldrich) by spin-coating. PMMA functioned as a supporting polymer layer. O_2 -plasma treatment using reactive ion etching (RIE) was performed to remove the graphene that had grown on the bottom of Cu foil. Then the foil was floated on ammonium persulfate (APS) solution (APS/DI water = 11 g/600 mL) for >5 h to etch away the Cu foil and then rinsed with deionized water for several hours to remove the etchant residue. The resulting floating single-layer graphene was transferred to the target substrate. The PMMA layer was removed by soaking in acetone bath and rinsing with acetone and isopropyl alcohol successively. By repeating this process four times, four-layer graphene (4LG) was stacked. Then 0.5 wt % N-DMBI in chlorobenzene was spin-cast to chemically dope the graphene, which was then annealed at 80 °C for 20 min.

Raman spectroscopy (WITEC) was performed with a 532 nm laser. Sheet resistance (R_{sh}) of graphene cathode was measured using a 4-point probe combined with a Keithley 2400 Source meter. Surface potential difference was measured using a SKP-5050 Kelvin Probe

measurement system. Optical transmittance (OT) was measured using a SCINCO S-3100 multichannel spectrophotometer.

All calculations in this work are performed using the planewave pseudopotential code VASP^{48–50} under the generalized gradient approximation of Perdew, Burke, and Ernzerhof (PBE).⁵¹ For atomic core-levels, we have used projected augmented wave (PAW) potentials^{52,53} treating the 2s2p of N and C, and 1s of H as the explicit valence electrons. A maximum energy cutoff of 400 eV is used for plane-wave basis set. In our calculations, the pure graphene has honeycomb lattice structure with triclinic unit cell and space group P1. For the combined graphene/dopant system, we have taken a supercell of graphene. The lattice constants of this hexagonal supercell are $a = b = 18.950 \text{ \AA}$, $c = 40.0 \text{ \AA}$, $a = b = 90^\circ$, and $g = 60^\circ$. There are in total 115 C, 33 H, and 3 N atoms in this supercell for graphene/DMBI system. We have relaxed our graphene/DMBI using van der Waals (vdW) interaction. To incorporate the vdW interaction, we have used optB86bvdW functional where the exchange functionals were optimized for the correlation part.⁵⁴ Therefore, the LDA correlation part present in the PBE functional is removed by using the parameter AGGAC = 0.000 in the input file in order to avoid double-counting.

The 4LG was patterned using O_2 plasma by RIE through a prepatterned shadow mask. ZnO precursor solution was prepared by dissolving 1.0 g of zinc acetate ($\text{Zn}(\text{CH}_3\text{COO})_2$, purchased from Sigma-Aldrich) and 0.28 g of ethanolamine in 5 mL of 2-methoxyethanol and 5 mL of methanol. Prepared ZnO precursor solution was stirred overnight. ZnO precursor solution was spin-cast at 1000 rpm for 60 s, then annealed at 150 °C for 1 h. Poly(ethyleneimine ethoxylated) (PEIE) solution was dissolved in 2-methoxyethanol (0.6 wt %) and spin-cast on the ZnO layer. Super yellow (PDY-132 from Merck) was dissolved in toluene (0.9 wt %) and spin-cast on the PEIE layer to form an emissive layer. MoO_3 (5 nm) and Ag (100 nm) were deposited on the emissive layer as an anode. The devices were encapsulated using a glass lid and epoxy resin. A Keithley 236 Source measurement unit and Minolta CS 2000 spectroradiometer were used to measure current–voltage–luminance characteristics of the PLEDs.

3. RESULTS AND DISCUSSION

We performed solution-processed n-type doping of graphene with N-DMBI, then used doped graphene as a cathode for inverted PLEDs (Figure 1). N-DMBI dopant solution was

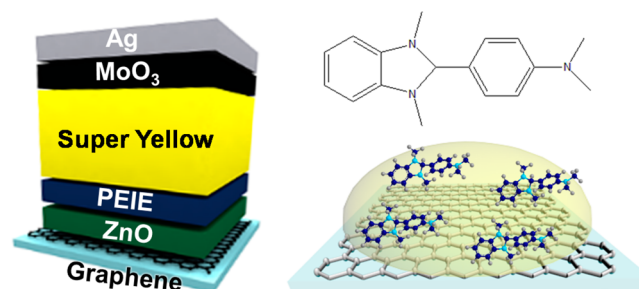


Figure 1. Schematics of inverted PLEDs with N-DMBI-doped graphene, and molecular structure of N-DMBI.

prepared by dissolving N-DMBI in chlorobenzene, then spin-cast on a graphene layer and thermally annealed to activate the N-DMBI molecules. Thermal annealing in N_2 atmosphere converts N-DMBI molecule to radical form. Although highest occupied molecular orbital level of N-DMBI is $\sim 4.67 \text{ eV}$, which does not allow spontaneous electron transfer to pristine graphene (WF $\sim 4.4 \text{ eV}$), N-DMBI radicals have singly occupied molecular orbital energy level of 2.36 eV and thus effectively induce n-type doping of graphene by spontaneously donating electron from N-DMBI radical to the graphene.⁵⁵ We used Raman spectroscopy as a nondestructive way to determine

the doping characteristics, and quality of graphene.^{56,57} Raman spectra of pristine and N-DMBI doped graphene showed clear G and 2D bands and an insignificant D-band (Figure 2a); that is, the graphene was successfully grown and transferred with high quality, and that the doping caused negligible defect generation.

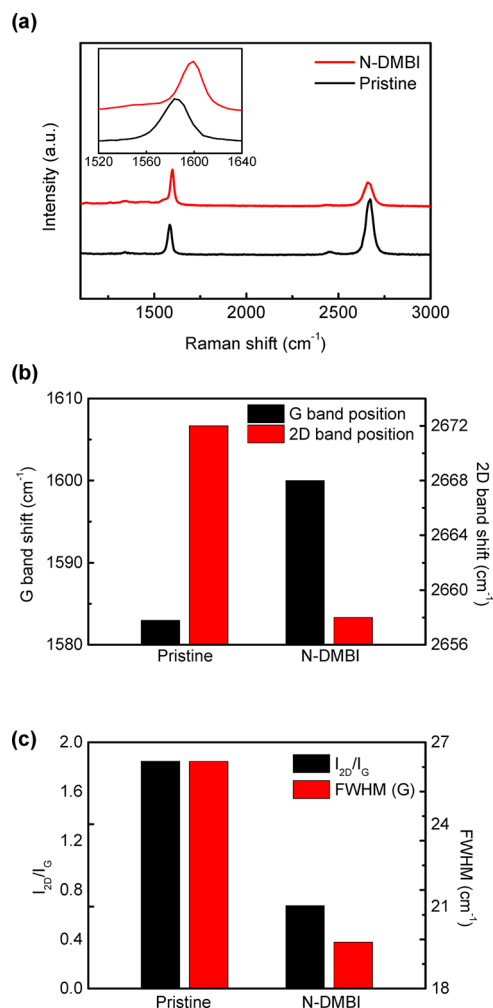


Figure 2. Raman spectrum of (a) average, (b) positions of G band and 2D band, and (c) intensity ratio of 2D band to G band, fwhm of G-band in pristine, and N-DMBI doped graphene.

Several attributes of Raman spectrum provide information about the doping state of graphene: (i) peak shift of G and 2D bands; (ii) changes of the ratio I_{2D}/I_G of the intensities of the 2D and G bands; and (iii) full width at half-maximum of the G band (fwhm(G)). N-type graphene doping shifts the characteristic peaks of graphene (upshifts the G-band peak and downshifts the 2D-band peak) and reduces I_{2D}/I_G and fwhm of G-bands.⁵⁶ N-type doping effect of graphene with various N-DMBI concentrations was investigated using Raman spectroscopy (Figure S1a). Raman spectrum of 0.5 wt % N-DMBI doped graphene exhibited clear downshift of 2D-band, which implies effective n-type doping on graphene. However, Raman spectrum of graphene doped with higher N-DMBI concentration (i.e., 1.0 wt %) showed almost identical shift of Raman bands with those of 0.5 wt %, which indicates that n-type doping effect by N-DMBI is saturated at > 0.5 wt %. Graphene doped with 1.0 wt % N-DMBI showed aggregation forming

large-sized particles, and it causes deleterious effects in both chemical doping and its devices (Figure S1b–e). 0.5 wt % of N-DMBI doped graphene showed upshift of G-band peak (pristine, 1583 cm⁻¹; N-DMBI, 1600 cm⁻¹) and downshift of 2D-band peak (pristine, 2672 cm⁻¹; N-DMBI, 2658 cm⁻¹) (Figure 2b). I_{2D}/I_G and fwhm of G-bands were both lower in N-DMBI doped graphene than in pristine graphene (I_{2D}/I_G of pristine, 1.846; N-DMBI, 0.674; fwhm(G) of pristine, 26.3 cm⁻¹, N-DMBI, 19.7 cm⁻¹) (Figure 2c). These results indicate that N-DMBI doped graphene showed effective n-type doping characteristics without degrading the quality of the graphene lattice. We performed X-ray photoelectron spectroscopy (XPS) to analyze the detailed chemical bonding characteristics of pristine and N-DMBI-doped graphene. In contrast to pristine graphene, N1s characteristic peak arises at binding energy of ~400 eV in N-DMBI doped graphene (Figure S2a).²⁸ C1s spectrum of N-DMBI doped graphene showed C–C sp² bonding (~284.7 eV), oxygen or nitrogen related carbon bondings (i.e., C–C sp³ or C–OH (~285.9 eV), C=O or C–N sp³ (~287.0 eV), and –C(O)O (~289.1 eV), which would come from wet-transfer residues (e.g., PMMA, isopropyl alcohol, acetone));^{7,40} these are similar to C1s spectrum of pristine graphene (Figure S2b). Deconvoluted peak at ~287.0 eV increased in C1s spectrum of N-DMBI doped graphene, which can attribute to the C–N sp³ chemical bonding from N-DMBI molecules (Figure S2c).⁵⁸

Kelvin probe measurements were performed to measure the surface WF changes caused by N-DMBI doping of four-layered graphene (4LG) (Figure 3a). N-DMBI doped 4LGs showed uniformly reduced WF by ~0.45 eV compared to the WF of pristine 4LG throughout the large area (2.54 × 2.54 mm²). Pristine graphene showed WF of 4.4 eV confirmed by ultraviolet photoelectron spectroscopy (Figure S3); these indicate that N-DMBI-doped 4LG has WF of 3.95 eV. OT change of the N-DMBI doped graphene indicated that N-DMBI doping does not significantly degrade the OT of pristine 4LG (pristine, 92.3%; N-DMBI, 89.5%) (Figure 3b).

Atomic-force microscopy (AFM) was performed to quantify how N-DMBI doping affected the surface morphology of 4LG (Figure S4). The pristine graphene surface was uniform (root-mean square (RMS) roughness $r = 1.61$ nm) throughout the area of 5 × 5 μm²; the heights of graphene wrinkles were < 5 nm. N-DMBI doped graphene surfaces were also uniform (N-DMBI: $r = 1.70$ nm) throughout the area of 5 × 5 μm² without any significant protruding regions along the surface; that is, N-DMBI doping does not cause any protruding regions on graphene, so that N-DMBI doped graphene can be applied in thin-film electronic devices.

To investigate the doping mechanism of N-DMBI on graphene, we performed density function theory (DFT) calculation on graphene and dopants (N-DMBI and its radical state). In our calculations, we have considered the N-DMBI and its radical where the missing H atom is indicated with the purple dot (Figure 4a). With detailed charge difference distribution ($\Delta\rho$), we can spatially visualize the characteristics of charge transfer (Figure 4b) between graphene and dopants. The charge density difference was obtained using the relation $\Delta\rho = \rho_{A+B} - \rho_A - \rho_B$. $\Delta\rho > 0$ tells us the excess electrons, which was described in yellow region. On the other hands, $\Delta\rho < 0$ is shown in blue region, which identifies the regions with electron deficiencies (e.g., holes) after the adsorption of the dopant took place. We can confirm no significant excess of electrons or equivalently lack of holes on graphene (blue cloud)

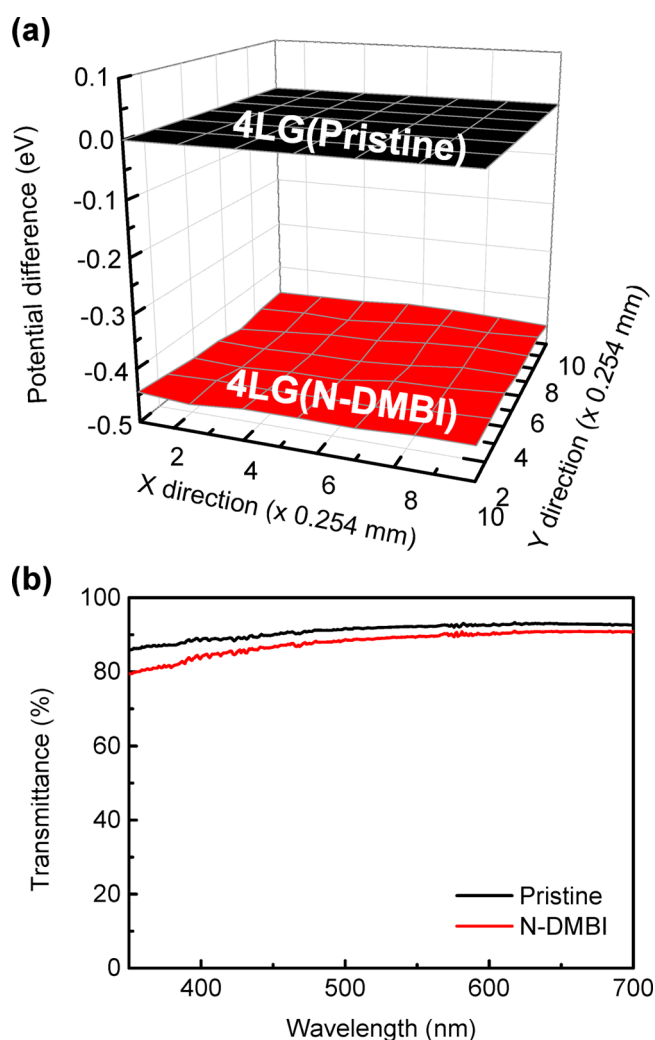


Figure 3. (a) Surface potential difference, (b) optical transmittance of pristine and N-DMBI doped 4LG.

in the vicinity of neutral N-DMBI. However, C atoms of graphene near the radical N-DMBI have excess of electrons (yellow cloud) in their p-orbitals. Density of state (DOS) of pristine, neutral N-DMBI doped, and radical N-DMBI doped graphene are presented (Figure 4c). Compared to pristine graphene, neutral N-DMBI doped graphene showed negligible n-type doping effect, while radical N-DMBI doped graphene showed clear n-type doping effect. We see the electron count of neutral N-DMBI doped graphene up to Fermi level for the nearest C atom and that of neutral N-DMBI doped graphene showed insignificant difference compared with that of the C atom in pristine graphene, while that of radical N-DMBI doped graphene is higher than pristine graphene (Figure 4d); this indicates neutral N-DMBI cannot act as effective electron donor, but radical N-DMBI acts as electron donor leaving the graphene n-doped. To summarize, N-DMBI doping on graphene provides several advantages for a transparent graphene cathode: (i) WF decrease (~ 0.45 eV), (ii) negligible defect generation, (iii) insignificant OT decrease, and (iv) smooth graphene surface.

We fabricated inverted PLEDs using pristine 4LG, and N-DMBI doped 4LG/ZnO (~ 120 nm)/PEIE (~ 8 nm)/Super Yellow (~ 230 nm)/MoO₃ (5 nm)/Ag (100 nm). We used metal oxide interfacial buffer layers that are air stable (i.e., ZnO

and MoO₃) for electron and hole injection, respectively. Even though N-DMBI doped graphene was followed by a solution-processed electron-injecting layer (ZnO), n-type doping effect of N-DMBI was still maintained, which was confirmed by Raman spectroscopy (Figure S5). We also investigated the electron-injecting properties of electron injecting interfacial layers (ZnO (120 nm)/PEIE (8 nm) or single PEIE (8 nm)) by fabricating the inverted PLEDs with [ITO/electron injecting interfacial layer/Super Yellow/MoO₃/Ag] (Figure S6). PLEDs using the ZnO/PEIE bilayers clearly showed improved current density and device efficiency than did those using single PEIE layer because conduction band minimum (CBM) of ZnO (~ 3.6 eV)²¹ is located between WF of n-typed graphene (~ 3.95 eV) and lowest unoccupied molecular orbital of Super Yellow (~ 3.0 eV). N-DMBI doping which can reduce the WF of graphene from 4.4 to 3.95 eV can efficiently reduce the electron injection barrier to the CBM (~ 3.6 eV) of ZnO and thus facilitate the electron injection during PLED operation (Figure 5a). The PLED with the N-DMBI-doped graphene showed a higher current density than that with pristine 4LG (Figure 5b). However, at high applied voltage > 20 V, the difference between current density of PLEDs with N-DMBI-doped 4LG and that with pristine 4LG decreased; this difference occurs because N-DMBI doped graphene has higher R_{sh} than does pristine 4LG (Figure S7) and because R_{sh} affects current density more than does WF in high voltage region.¹⁴ Pristine 4LGs have inherent p-type doped properties owing to the residual etchant, adsorbed H₂O, O₂, or PMMA residue.^{1,38,40} N-DMBI doping reduces the residual p-type doping effect of pristine 4LG, and thereby decreases the hole concentration and increases the R_{sh} of pristine 4LG (as-transferred: 185.8 Ω/sq , N-DMBI doped: 537.5 Ω/sq). To investigate the pure n-type doping effect of N-DMBI on pristine graphene, we annealed the pristine 4LG in vacuum chamber at 500 $^{\circ}\text{C}$ for 3 h to remove the residual p-type dopants, then doped it with N-DMBI. R_{sh} was increased by ~ 8 times due to removal of residual p-type dopants (pristine 4LG, 202.1 Ω/sq ; annealed 4LG, 1632 Ω/sq); N-DMBI doping on the annealed graphene decreased its R_{sh} by $\sim 35\%$. The high WF of pristine 4LG obstructs electron injection and increased the operating voltage, whereas N-DMBI doped 4LG provided efficient electron injection between a graphene cathode and an overlying ZnO layer by reducing the WF of graphene. As a result, N-DMBI doped graphene exhibited lower operating voltage than that of pristine graphene (Figure 5c), and PLEDs with N-DMBI doped 4LGs showed higher current efficiency (CE) than PLEDs with pristine 4LGs (pristine, 2.74 cd/A; N-DMBI, 13.8 cd/A) (Figure 5d). N-DMBI doping decreased the electron injection energy barrier and provided an improved electron–hole balance, which resulted in a higher luminous efficiency. Simple solution-process N-DMBI doping on graphene substantially increased the luminous characteristics of PLEDs.

4. CONCLUSION

We have investigated the effect of n-type doping in graphene using N-DMBI, then used the doped graphene as a transparent cathode in PLEDs. Both experimental and computational analyses confirmed that N-DMBI doped graphene can be a promising cathode in organic optoelectronics. N-DMBI doping reduced the WF of pristine graphene by ~ 0.45 eV without structural defects, nor large particles on its surface. N-DMBI doping reduced the OT of 4LG by $< 3\%$. Use of N-DMBI-

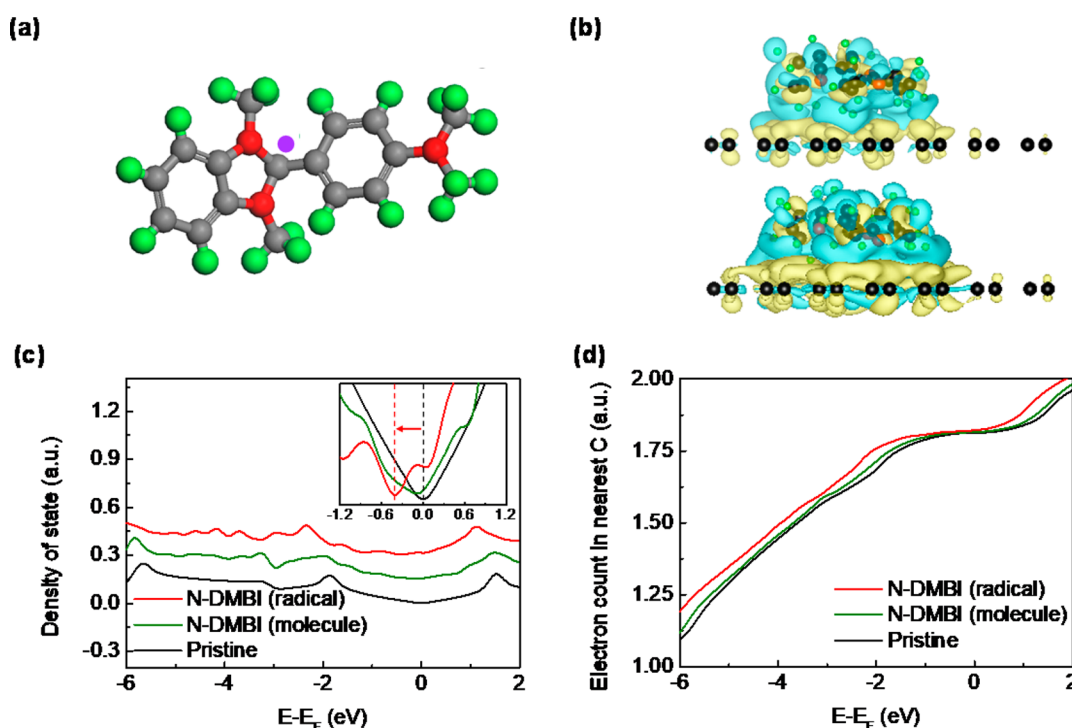


Figure 4. (a) Molecular structures of radical N-DMBI. The purple dot on N-DMBI radical indicates the missing H atom, which occurred in thermal annealing. Spheres: red = nitrogen, gray = carbon, green = hydrogen. (b) Spatial distribution of charge density difference in N-DMBI dopant and graphene (top, neutral N-DMBI; bottom, radical N-DMBI), (c) density of state, and (d) electron count at the C atom of nearest to the N-DMBI (green, graphene + neutral N-DMBI; red, graphene + radical N-DMBI), and pristine graphene (black). Black and red vertical dashed lines in inset of (c) correspondingly shows the Dirac points of pristine graphene and graphene + N-DMBI (radical) complex.

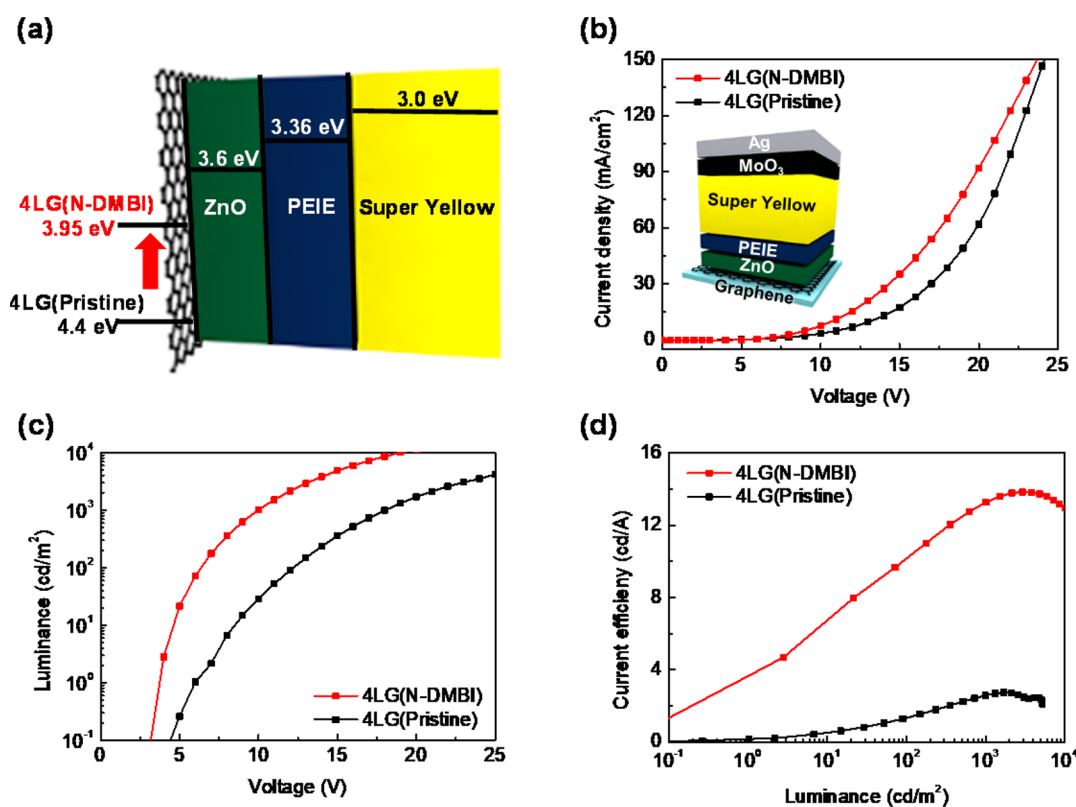


Figure 5. (a) Schematic diagram of inverted PLEDs with pristine or N-DMBI doped 4LG, (b) current densities, (c) luminances, and (d) current efficiencies of inverted PLEDs using pristine or N-DMBI doped 4LG.

doped 4LG cathodes in PLEDs reduced their operating voltage and considerably improved their luminous efficiency (13.8 cd/A), because N-DMBI doped graphene significantly improved the electron injection properties due to substantially reduced electron injection barrier from the graphene to an overlying ZnO layer. n-Type graphene doping by solution process using N-DMBI simply and effectively decreased the WF of graphene. This method provide an important step toward high-efficiency inverted PLEDs using graphene cathodes, which can be potentially used for future flexible and stretchable displays. This result can expand the utility of solution-processed graphene doping in use of electrodes for high-efficiency OLEDs which has been previously biased toward p-type doping for anode, to n-type doping for cathode.

■ ASSOCIATED CONTENT

Supporting Information

The Supporting Information is available free of charge on the ACS Publications website at DOI: 10.1021/acsami.7b15307.

Physical and chemical properties changes of N-DMBI doping on graphene, optical microscopy and atomic force microscopy images of pristine, and n-doped graphene, and luminous properties of inverted PLEDs with varying electron injecting interfacial interlayer on inverted PLEDs (PDF)

■ AUTHOR INFORMATION

Corresponding Author

*E-mail: twlees@snu.ac.kr; taewlees@gmail.com.

ORCID

Byung Hee Hong: 0000-0001-8355-8875

Jian-Xin Zhu: 0000-0001-7991-3918

Tae-Woo Lee: 0000-0002-6449-6725

Author Contributions

◆S.-J.K., T.-H.H., and Y.-H.K. contributed equally to this work.

Notes

The authors declare no competing financial interest.

■ ACKNOWLEDGMENTS

This work was supported by the National Research Foundation of Korea (NRF) grant funded by the Korea government (MSIT) (NRF-2016R1A3B1908431). Also, this work was supported by the National Research Foundation of Korea (NRF) grant funded by the Korea government (Ministry of Science, ICT & Future Planning) (NRF-2017R1C1B2009161). This work was in part supported by the Center for Integrated Nanotechnologies, a U.S. DOE Basic Energy Science user facility.

■ REFERENCES

- (1) Novoselov, K. S.; Geim, A. K.; Morozov, S. V.; Jiang, D.; Zhang, Y.; Dubonos, S. V.; Grigorieva, I. V.; Firsov, A. A. Electric Field Effect in Atomically Thin Carbon Films. *Science* **2004**, *306*, 666–669.
- (2) Kim, K. S.; Zhao, Y.; Jang, H.; Lee, S. Y.; Kim, J. M.; Kim, K. S.; Ahn, J.-H.; Kim, P.; Choi, J.-Y.; Hong, B. H. Large-Scale Pattern Growth of Graphene Films for Stretchable Transparent Electrodes. *Nature* **2009**, *457*, 706–710.
- (3) Bae, S.; Kim, H.; Lee, Y.; Xu, X.; Park, J.-S.; Zheng, Y.; Balakrishnan, J.; Lei, T.; Kim, H. R.; Song, Y. I.; Kim, Y.-J.; Kim, K. S.; Özyilmaz, B.; Ahn, J.-H.; Hong, B. H.; Iijima, S. Roll-to-roll production of 30-in. graphene films for transparent electrodes. *Nat. Nanotechnol.* **2010**, *5*, 574–578.
- (4) Geim, A. K.; Novoselov, K. S. The rise of graphene. *Nat. Mater.* **2007**, *6*, 183–191.
- (5) Li, X.; Cai, W.; An, J.; Kim, S.; Nah, J.; Yang, D.; Piner, R.; Velamakanni, A.; Jung, I.; Tutuc, E.; Banerjee, S. K.; Colombo, L.; Ruoff, E. S. Large-Area Synthesis of High-Quality and Uniform Graphene Films on Copper Foils. *Science* **2009**, *324*, 1312–1314.
- (6) Cho, H.; Kim, S. D.; Han, T.-H.; Song, I.; Byun, J.-W.; Kim, Y.-H.; Kwon, S.; Bae, S.-H.; Choi, H. C.; Ahn, J.-H.; Lee, T.-W. Improvement of work function and hole injection efficiency of graphene anode using CHF₃ plasma treatment. *2D Mater.* **2015**, *2*, 014002.
- (7) Han, T.-H.; Kwon, S.-J.; Seo, H.-K.; Lee, T.-W. Controlled surface oxidation of multi-layered graphene anode to increase hole injection efficiency in organic electronic devices. *2D Mater.* **2016**, *3*, 014003.
- (8) Han, T.-H.; Kim, H.; Kwon, S.-J.; Lee, T.-W. Graphene-based flexible electronic devices. *Mater. Sci. Eng., R* **2017**, *118*, 1–44.
- (9) Han, T.-H.; Lee, Y.; Choi, M.-R.; Woo, S.-H.; Bae, S.-H.; Hong, B. H.; Ahn, J.-H.; Lee, T.-W. Extremely efficient flexible organic light-emitting diodes with modified graphene anode. *Nat. Photonics* **2012**, *6*, 105–110.
- (10) Li, N.; Oida, S.; Tulevski, G. S.; Han, S.-J.; Hannon, J. B.; Sadana, D. K.; Chen, T.-C. Efficient and bright organic light-emitting diodes on single-layer graphene electrodes. *Nat. Commun.* **2013**, *4*, 2294.
- (11) Kim, D.; Lee, D.; Lee, Y.; Jeon, D. Y. Work-Function Engineering of Graphene Anode by Bis(trifluoromethanesulfonyl)-amide Doping for Efficient Polymer Light-Emitting Diodes. *Adv. Funct. Mater.* **2013**, *23*, 5049–5055.
- (12) Meyer, J.; Kidambi, P. R.; Bayer, B. C.; Weijtens, C.; Kuhn, A.; Centeno, A.; Pesquera, A.; Zurutuza, A.; Robertson, J.; Hofmann, S. Metal Oxide Induced Charge Transfer Doping and Band Alignment of Graphene Electrodes for Efficient Organic Light Emitting Diodes. *Sci. Rep.* **2015**, *4*, 5380.
- (13) Sanders, S.; Cabrero-Vilatela, A.; Kidambi, P. R.; Alexander-Webber, J. A.; Weijtens, C.; Braeuninger-Weimer, P.; Aria, A. I.; Qasim, M. M.; Wilkinson, T. D.; Robertson, J.; Hofmann, S.; Meyer, J. Engineering high charge transfer n-doping of graphene electrodes and its application to organic electronics. *Nanoscale* **2015**, *7*, 13135–13142.
- (14) Hwang, J. O.; Park, J. S.; Choi, D. S.; Kim, J. Y.; Lee, S. H.; Lee, K. E.; Kim, Y.-H.; Song, M. H.; Yoo, S.; Kim, S. O. Workfunction-Tunable, N-Doped Reduced Graphene Transparent Electrodes for High-Performance Polymer Light-Emitting Diodes. *ACS Nano* **2012**, *6*, 159–167.
- (15) Han, T.-H.; Kwon, S.-J.; Li, N.; Seo, H.-K.; Xu, W.; Kim, K. S.; Lee, T.-W. Versatile p-Type Chemical Doping to Achieve Ideal Flexible Graphene Electrodes. *Angew. Chem., Int. Ed.* **2016**, *55*, 6197–6201.
- (16) Han, T.-H.; Park, M.-H.; Kwon, S.-J.; Bae, S.-H.; Seo, H.-K.; Cho, H.; Ahn, J.-H.; Lee, T.-W. Approaching Ultimate Flexible Organic Light-Emitting Diodes Using Graphene Anode. *NPG Asia Mater.* **2016**, *8*, e303.
- (17) Lee, J.; Han, T.-H.; Park, M.-H.; Jung, D. Y.; Seo, J.; Seo, H.-K.; Cho, H.; Kim, E.; Chung, J.; Choi, S.-Y.; Kim, T.-S.; Lee, T.-W.; Yoo, S. Synergetic electrode architecture for efficient graphene-based flexible organic light-emitting diodes. *Nat. Commun.* **2016**, *7*, 11791.
- (18) Wang, Y.; Tong, S. W.; Xu, X. F.; Özyilmaz, B.; Loh, K. P. Interface Engineering of Layer-by-Layer Stacked Graphene Anodes for High-Performance Organic Solar Cells. *Adv. Mater.* **2011**, *23*, 1514–1518.
- (19) Kim, H.; Bae, S.-H.; Han, T.-H.; Lim, K.-G.; Ahn, J.-H.; Lee, T.-W. Organic solar cells using CVD-grown graphene electrodes. *Nanotechnology* **2014**, *25*, 014012.
- (20) Kim, K.; Bae, S.-H.; Toh, C. T.; Kim, H.; Cho, J. H.; Whang, D.; Lee, T.-W.; Özyilmaz, B.; Ahn, J.-H. Ultrathin Organic Solar Cells with Graphene Doped by Ferroelectric Polarization. *ACS Appl. Mater. Interfaces* **2014**, *6*, 3299–3304.

- (21) Kim, H.; Byun, J.; Bae, S.-H.; Ahmed, T.; Zhu, J.-X.; Kwon, S.-J.; Lee, Y.; Min, S.-Y.; Wolf, C.; Seo, H.-K.; Ahn, J.-H.; Lee, T.-W. On-Fabrication Solid-State N-Doping of Graphene by an Electron-Transporting Metal Oxide Layer for Efficient Inverted Organic Solar Cells. *Adv. Energy Mater.* **2016**, *6*, 1600172.
- (22) Van Le, Q.; Choi, J.-Y.; Kim, S. Y. Recent advances in the application of two-dimensional materials as charge transport layers in organic and perovskite solar cells. *FlatChem.* **2017**, *2*, 54–66.
- (23) Park, J.; Lee, W. H.; Huh, S.; Sim, S. H.; Kim, S. B.; Cho, K.; Hong, B. H.; Kim, K. S. Work-Function Engineering of Graphene Electrodes by Self-Assembled Monolayers for High-Performance Organic Field-Effect Transistors. *J. Phys. Chem. Lett.* **2011**, *2*, 841–845.
- (24) Liu, W.; Jackson, B. L.; Zhu, J.; Miao, C.-Q.; Chung, C.-H.; Park, Y.-J.; Sun, K.; Woo, J.; Xie, Y.-H. Large Scale Pattern Graphene Electrode for High Performance in Transparent Organic Single Crystal Field-Effect Transistors. *ACS Nano* **2010**, *4*, 3927–3932.
- (25) Wei, D.; Liu, Y.; Wang, Y.; Zhang, H.; Huang, L.; Yu, G. Synthesis of N-Doped Graphene by Chemical Vapor Deposition and Its Electrical Properties. *Nano Lett.* **2009**, *9*, 1752–1758.
- (26) Guo, B.; Liu, Q.; Chen, E.; Zhu, H.; Fang, L.; Gong, J. R. Controllable N-Doping of Graphene. *Nano Lett.* **2010**, *10*, 4975–4980.
- (27) Panchakarla, L. S.; Subrahmanyam, K. S.; Saha, S. K.; Govindaraj, A.; Krishnamurthy, H. R.; Waghmare, U. V.; Rao, C. N. R. Synthesis, Structure, and Properties of Boron- and Nitrogen-Doped Graphene. *Adv. Mater.* **2009**, *21*, 4726–4730.
- (28) Park, S.; Hu, Y.; Hwang, J. O.; Lee, E.-S.; Casabianca, L. B.; Cai, W.; Potts, J. R.; Ha, H.-W.; Chen, S.; Oh, J.; Kim, S. O.; Kim, Y.-H.; Ishii, Y.; Ruoff, R. S. Chemical structures of hydrazine-treated graphene oxide and generation of aromatic nitrogen doping. *Nat. Commun.* **2012**, *3*, 638.
- (29) Denis, P. A. Band gap opening of monolayer and bilayer graphene doped with aluminium, silicon, phosphorus, and sulfur. *Chem. Phys. Lett.* **2010**, *492*, 251–257.
- (30) Some, S.; Bhunia, P.; Hwang, E.; Lee, K.; Yoon, Y.; Seo, S.; Lee, H. Can Commonly Used Hydrazine Produce n-Type Graphene? *Chem. - Eur. J.* **2012**, *18*, 7665–7670.
- (31) Wang, X.; Li, X.; Zhang, L.; Yoon, Y.; Weber, P. K.; Wang, H.; Guo, J.; Dai, H. N-Doping of Graphene Through Electrothermal Reactions with Ammonia. *Science* **2009**, *324*, 768–771.
- (32) Xu, W.; Lim, T.-S.; Seo, H.-K.; Min, S.-Y.; Cho, H.; Park, M.-H.; Kim, Y.-H.; Lee, T.-W. N-Doped Graphene Field-Effect Transistors with Enhanced Electron Mobility and Air-Stability. *Small* **2014**, *10*, 1999–2005.
- (33) Xu, W.; Wang, L.; Liu, Y.; Thomas, S.; Seo, H.-K.; Kim, K.-I.; Kim, K. S.; Lee, T.-W. Controllable n-Type Doping on CVD-Grown Single- and Double-Layer Graphene Mixture. *Adv. Mater.* **2015**, *27*, 1619–1623.
- (34) Wei, P.; Liu, N.; Lee, H. R.; Adijanto, E.; Ci, L.; Naab, B. D.; Zhong, J. Q.; Park, J.; Chen, W.; Cui, Y.; Bao, Z. Tuning the Dirac Point in CVD-Grown Graphene through Solution Processed n-Type Doping with 2-(2-Methoxyphenyl)-1,3-dimethyl-2,3-dihydro-1H-benzimidazole. *Nano Lett.* **2013**, *13*, 1890–1897.
- (35) Ho, P.-H.; Yeh, Y.-C.; Wang, D.-Y.; Li, S.-S.; Chen, H.-A.; Chung, Y.-H.; Lin, C.-C.; Wang, W.-H.; Chen, C.-W. Self-Encapsulated Doping of n-Type Graphene Transistors with Extended Air Stability. *ACS Nano* **2012**, *6*, 6215–6221.
- (36) Maiti, U. N.; Lee, W. J.; Lee, J. M.; Oh, Y.; Kim, J. Y.; Kim, J. E.; Shim, J.; Han, T. H.; Kim, S. O. 25th Anniversary Article: Chemically Modified/Doped Carbon Nanotubes & Graphene for Optimized Nanostructures & Nanodevices. *Adv. Mater.* **2014**, *26*, 40–67.
- (37) Lee, W. J.; Maiti, U. N.; Lee, J. M.; Lim, J.; Han, T. H.; Kim, S. O. Nitrogen-doped carbon nanotubes and graphene composite structures for energy and catalytic applications. *Chem. Commun.* **2014**, *50*, 6818–6830.
- (38) Cheng, Z.; Zhou, Q.; Wang, C.; Li, Q.; Wang, C.; Fang, Y. Toward Intrinsic Graphene Surfaces: A Systematic Study on Thermal Annealing and Wet-Chemical Treatment of SiO₂-Supported Graphene Devices. *Nano Lett.* **2011**, *11*, 767–771.
- (39) Ryu, S.; Liu, L.; Berciaud, S.; Yu, Y.-J.; Liu, H.; Kim, P.; Flynn, G. W.; Brus, L. E. Atmospheric Oxygen Binding and Hole Doping in Deformed Graphene on a SiO₂ Substrate. *Nano Lett.* **2010**, *10*, 4944–4951.
- (40) Pirkle, A.; Chan, J.; Venugopal, A.; Hinojos, D.; Magnuson, C. W.; McDonnell, S.; Colombo, L.; Vogel, E. M.; Ruoff, R. S.; Wallace, R. M. The Effect of Chemical Residues on the Physical and Electrical Properties of Chemical Vapor Deposited Graphene Transferred to SiO₂. *Appl. Phys. Lett.* **2011**, *99*, 122108.
- (41) Lv, R.; Li, Q.; Botello-Méndez, A. R.; Hayashi, T.; Wang, B.; Berkdemir, A.; Hao, Q.; Elías, A. L.; Cruz-Silva, R.; Gutiérrez, H. R.; Kim, Y. A.; Muramatsu, H.; Zhu, J.; Endo, M.; Terrones, H.; Charlier, J.-C.; Pan, M.; Terrones, M. Nitrogen-doped graphene: beyond single substitution and enhanced molecular sensing. *Sci. Rep.* **2012**, *2*, 586.
- (42) Romero, H. E.; Joshi, P.; Gupta, A. K.; Gutierrez, H. R.; Cole, M. W.; Tadigadapa, S. A.; Eklund, P. C. Adsorption of ammonia on graphene. *Nanotechnology* **2009**, *20*, 245501.
- (43) Kim, Y.-H.; Han, T.-H.; Cho, H.; Min, S.-Y.; Lee, C.-L.; Lee, T.-W. Polyethylene Imine as an Ideal Interlayer for Highly Efficient Inverted Polymer Light-Emitting Diodes. *Adv. Funct. Mater.* **2014**, *24*, 3808–3814.
- (44) Bolink, H. J.; Coronado, E.; Repetto, D.; Sessolo, M. Air stable hybrid organic-inorganic light emitting diodes using ZnO as the cathode. *Appl. Phys. Lett.* **2007**, *91*, 223501.
- (45) Kabra, D.; Song, M. H.; Wenger, B.; Friend, R. H.; Snaith, H. J. High Efficiency Composite Metal Oxide-Polymer Electroluminescent Devices: A Morphological and Material Based Investigation. *Adv. Mater.* **2008**, *20*, 3447–3452.
- (46) Park, J. S.; Lee, B. R.; Jeong, E.; Lee, H.-J.; Lee, J. M.; Kim, J.-S.; Kim, J. Y.; Woo, H. Y.; Kim, S. O.; Song, M. H. High performance polymer light-emitting diodes with N-type metal oxide/conjugated polyelectrolyte hybrid charge transport layers. *Appl. Phys. Lett.* **2011**, *99*, 163305.
- (47) Lee, B. R.; Jung, E. D.; Park, J. S.; Nam, Y. S.; Min, S. H.; Kim, B.-S.; Lee, K.-M.; Jeong, J.-R.; Friend, R. H.; Kim, J.-S.; Kim, S. O.; Song, M. H. Highly efficient inverted polymer light-emitting diodes using surface modifications of ZnO layer. *Nat. Commun.* **2014**, *5*, 4840.
- (48) Kresse, G.; Furthmüller, J. Efficient iterative schemes for ab initio total-energy calculations using a plane-wave basis set. *Phys. Rev. B: Condens. Matter Mater. Phys.* **1996**, *54*, 11169–11186.
- (49) Kresse, G.; Hafner, J. Ab initio molecular dynamics for liquid metals. *Phys. Rev. B: Condens. Matter Mater. Phys.* **1993**, *47*, 558–561.
- (50) Kresse, G.; Furthmüller, J. Efficiency of ab-initio total energy calculations for metals and semiconductors using a plane-wave basis set. *Comput. Mater. Sci.* **1996**, *6*, 15–50.
- (51) Perdew, J. P.; Burke, K.; Ernzerhof, M. Generalized Gradient Approximation Made Simple. *Phys. Rev. Lett.* **1996**, *77*, 3865–3868.
- (52) Vanderbilt, D. Soft self-consistent pseudopotentials in a generalized eigenvalue formalism. *Phys. Rev. B: Condens. Matter Mater. Phys.* **1990**, *41*, 7892–7895.
- (53) Kresse, G.; Hafner, J. Norm-conserving and ultrasoft pseudopotentials for first-row and transition elements. *J. Phys.: Condens. Matter* **1994**, *6*, 8245.
- (54) Klimeš, J.; Bowler, D. R.; Michaelides, A. Van der Waals density functionals applied to solids. *Phys. Rev. B: Condens. Matter Mater. Phys.* **2011**, *83*, 195131.
- (55) Wei, P.; Oh, J. H.; Dong, G.; Bao, Z. Use of a 1H-Benzimidazole Derivative as an n-Type Dopant and To Enable Air-Stable Solution-Processed n-Channel Organic Thin-Film Transistors. *J. Am. Chem. Soc.* **2010**, *132*, 8852–8853.
- (56) Das, A.; Pisana, S.; Chakraborty, B.; Piscanec, S.; Saha, S. K.; Waghmare, U. V.; Novoselov, K. S.; Krishnamurthy, H. R.; Geim, A. K.; Ferrari, A. C.; et al. Monitoring Dopants by Raman Scattering in an Electrochemically Top-Gated Graphene Transistor. *Nat. Nanotechnol.* **2008**, *3*, 210–215.
- (57) Ferrari, A. C.; Meyer, J. C.; Scardaci, V.; Casiraghi, C.; Lazzeri, M.; Mauri, F.; Piscanec, S.; Jiang, D.; Novoselov, K. S.; Roth, S.; Geim, A. K. Raman Spectrum of Graphene and Graphene Layers. *Phys. Rev. Lett.* **2006**, *97*, 187401.

(58) Wang, C.; Cao, X.; Bourgeois, L.; Guan, H.; Chen, S.; Zhong, Y.; Tang, D.-M.; Li, H.; Zhai, T.; Li, L.; Bando, Y.; Golberg, D. N-Doped Graphene-SnO₂ Sandwich Paper for High-Performance Lithium-Ion Batteries. *Adv. Funct. Mater.* **2012**, 22, 2682–2690.